Supplementary Information

Introducing paired electric dipole layers for efficient and reproducible perovskite solar cells

*Jong-Hoon Lee†, Junghwan Kim†, Geunjin Kim, Dongguen Shin, Song Yi Jeong, Jinho Lee, Soonil Hong, Jin Woo Choi, Chang-Lyoul Lee, Heejoo Kim, Yeonjin Yi, and Kwanghee Lee**

Contents

1. Preparation of p-PFP-O

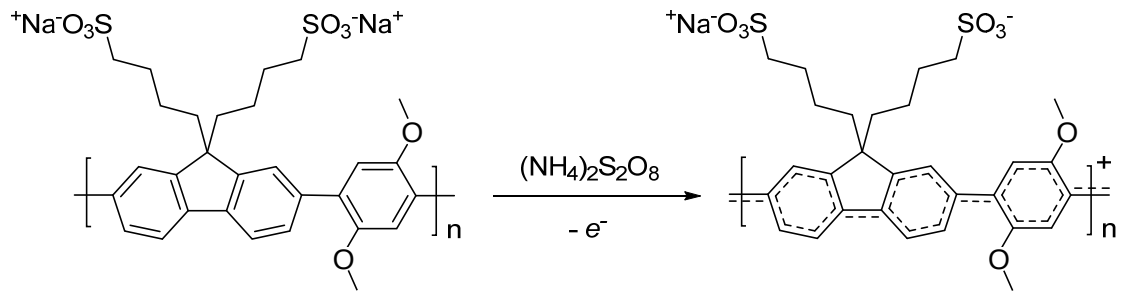

PFP-O **p-PFP-O**

Scheme S1. Preparation of p-PFP-O: oxidative treatment of conventional PFP-O with ammonium persulfate salts $(NH_4)_2S_2O_8$. The details of the preparation of p-doped CPEs are well described in our previous works.[1,2]

2. WF tunability of EDLs and CTLs

Table S1. The effective changes in the WF of ITO before and after interlayer deposition.

	Material	ΔWF (eV)
	ITO	0 (4.8)
CTL	PEDOT:PSS	+0.40
	TiO_x	-0.40
EDL	p-PFP-O	+0.60
	PFN	-0.60

Table S2. The effective changes in the WF of ITO/$PC_{61}BM$ before and after EEL deposition.

Material	ΔWF (eV)
(ITO/$PC_{61}BM$)	0 (4.9)
TiO_x	-0.40
PFN	-0.50

3. Surface potential and AFM topographic images

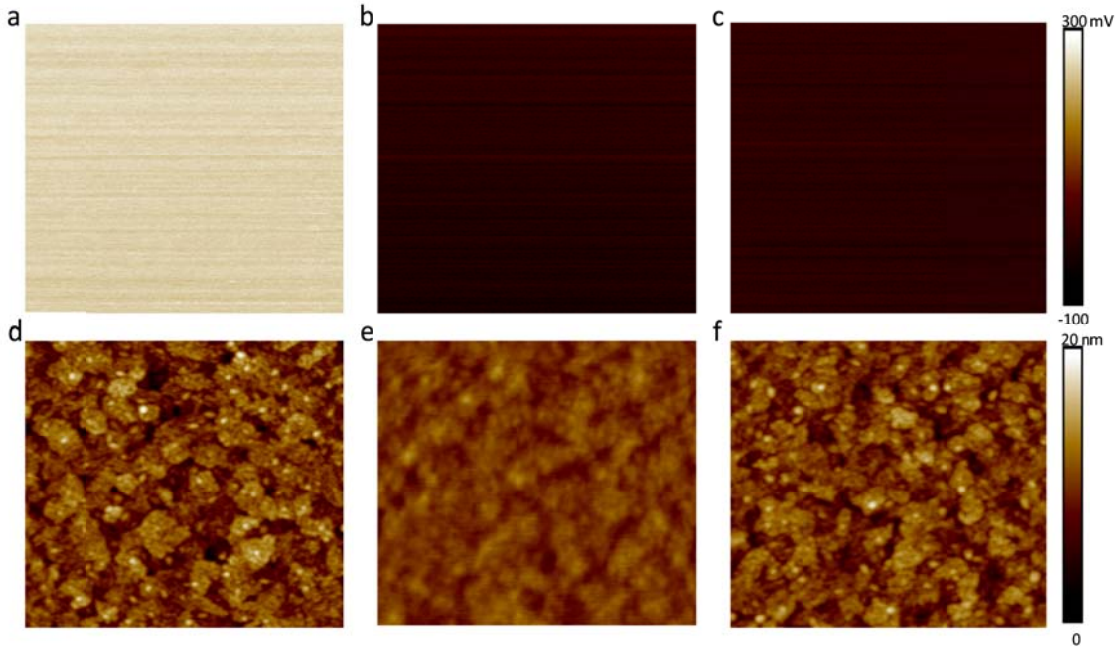

Figure S1. Surface potential (a-c) and AFM topographic images (d-f) of ITO (a,d), ITO/PEDOT:PSS (b,e) and ITO/p-PFP-O (c,f). (Scan size: 2 μm × 2 μm)

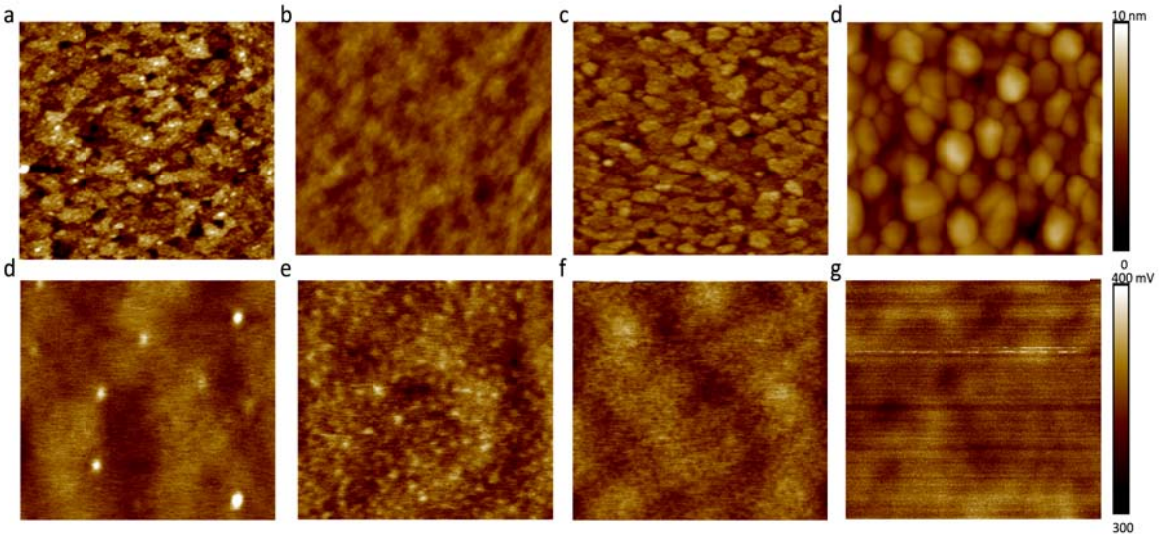

Figure S2. AFM topographic images of PTAA (a-c) on ITO, ITO/PEDOT:PSS and ITO/p-PFP-O, and (d-f) $MAPbI_3$, $MAPbI_3/PC_{61}BM$/, $MAPbI_3/PC_{61}BM/TiO_x$, $MAPbI_3/PC_{61}BM$/PFN. (g) Surface potential image of perovskite film (d). (Scan size: 2 μm × 2 μm)

4. Sample preparation process using a detaching method

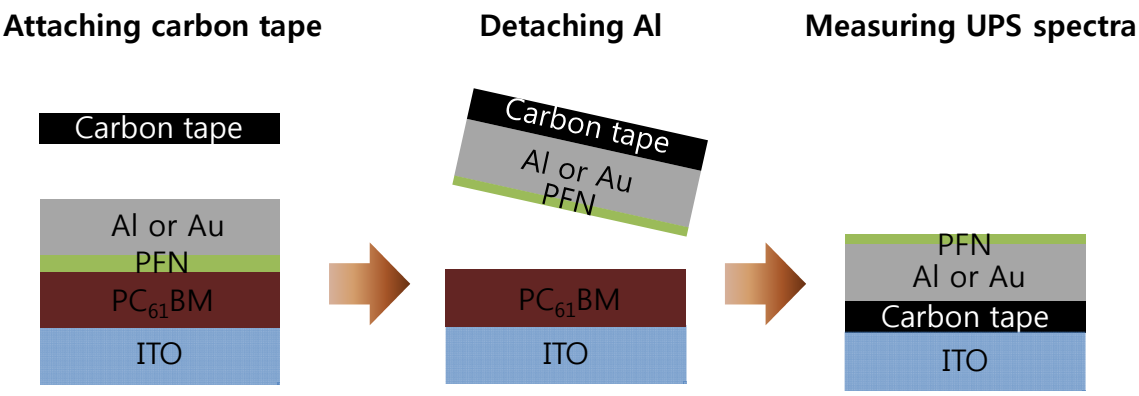

Figure S3. Schematic illustration of the sample preparation for UPS. The procedure for the sample preparation is as follows; 1) Attaching carbon tape on the devices with structures of ITO/PC_{61}BM/Al (or Au) and ITO/PC_{61}BM/PFN/Al (or Au), 2) detaching carbon tape from the devices, 3) attaching the detached samples on ITO.

5. UPS spectra of PFN and Au/PFN

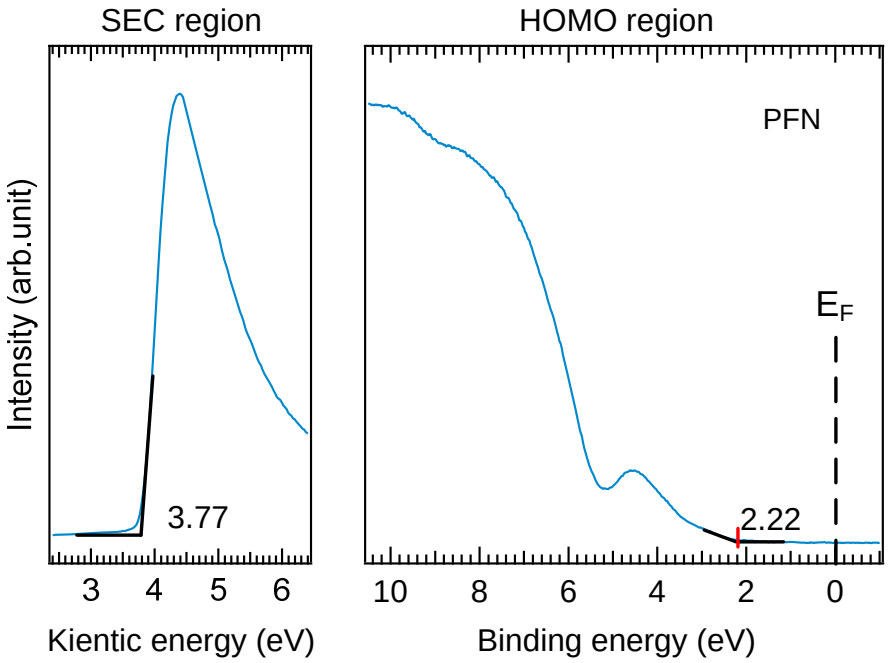

Figure S4. UPS spectra obtained from ITO/PFN.

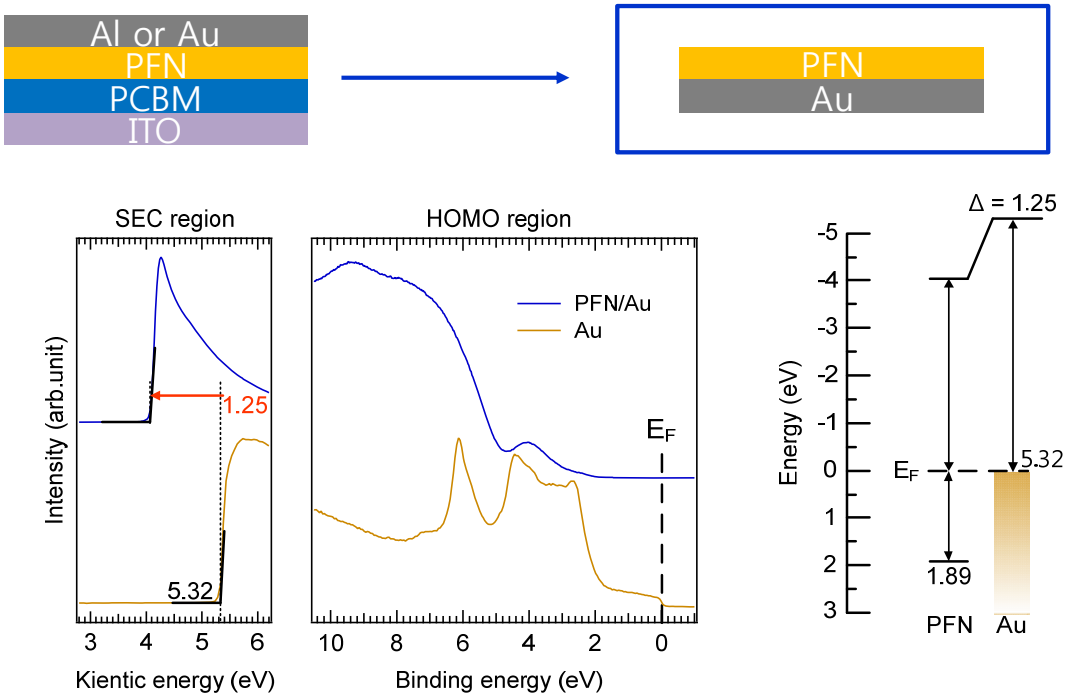

Figure S5. UPS spectra obtained from Au/PFN~ and their corresponding energy level diagram.

6. PeSC device performance

Table S3. Performance parameters of PeSCs measured under forward and reverse bias sweep.

	Direction	V_{oc} (V)	J_{sc} (mA cm^{-2})	FF	PCE (%)
No interlayers	Forward	1.11	19.2	0.68	14.5
	Reverse	1.11	19.3	0.69	14.7
CTLs	Forward	1.07	20.6	0.79	17.6
	Reverse	1.08	20.7	0.80	17.8
EDLs	Forward	1.10	21.4	0.81	19.1
	Reverse	1.10	21.5	0.82	19.4

Table S4. Performance parameters of PeSCs with PEDOT:PSS or p-PFP-O as the HEL and TiO_x or PFN as the EEL. All reported solar cell parameters are the averaged values achieved among 40 devices of each type. The numbers in parentheses are the average values (± standard deviation) for all devices.

HEL	EEL	V_{oc} (V)	J_{sc} (mA cm^{-2})	FF	PCE (%)	R_s (Ω cm^2)	R_{sh} ($\times 10^3$ Ω cm^2)
PEDOT:PSS	TiO_x	1.07±0.01	19.3±1.0	0.76±0.02	15.6±1.05	7.8±0.9	2.4±1.1
p-PFP-O	PFN	1.09±0.01	20.8±0.8	0.79±0.01	18.0±0.70	7.0±0.9	4.2±1.5

7. EQE spectra of PeSCs

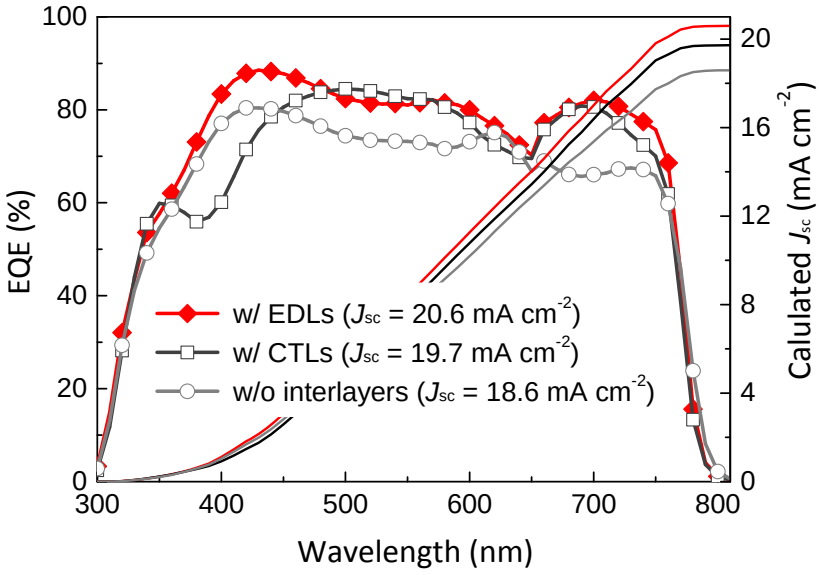

Figure S6. EQE spectra of the PeSCs without interlayers and with paired EDLs or CTLs.

8. *J-V* characteristics of PeSCs

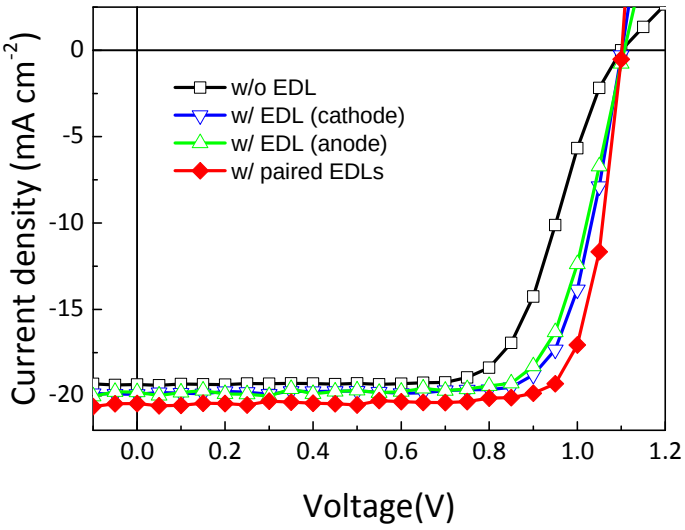

Figure S7. *J-V* characteristics of PeSCs without EDLs, with only one EDL or paired EDLs.

Table S5. Performance parameters of PeSCs measured under forward and reverse bias sweep.

Condition	V_{oc} (V)	J_{sc} (mA cm^{-2})	FF	PCE (%)
w/o ELDs	1.10	18.9	0.69	14.3
w/ EDL (anode)	1.10	20.3	0.77	17.2
w/ EDL (cathode)	1.10	20.4	0.76	17.1
w/ paired EDLs	1.10	21.5	0.82	19.4

9. Photoluminescence of PeSCs

Steady-state photoluminescence (PL) spectra of PeSC devices with and without the paired EDLs were obtained by using a monochromators (SP-2150i, Acton) equipped with photomultiplier tube (PMT, Acton PD471) and pulsed diode-laser head (LDH-P-C-405, PicoQuant) as an excitation source.

Time-resolved PL measurements were conducted using a time-correlated single photon counting setup (PicoQuant, Germany) with a 400 nm picosecond pulsed laser source (LDH-P-C-405, PicoQuant) and laser-diode driver (PDL 800-B, PicoQuant). The 700nm photon emission was resolved using a monochromators (SP-2150i, Acton) and its time-resolved characteristic was measured by using a TCSPC module (PicoHarp 260, PicoQuant) with a micro channel plate photomultiplier tube (MCP-PMT, R3809U-59, Hamamatsu).

Figure S8 (a) shows steady state PL spectra of perovskite layer and the PeSCs devices with and without EDLs under short circuit condition. We observed that steady state PL intensity was clearly reduced when the paired EDLs were introduced in PeSC devices. Furthermore, from the time-resolved PL decay measurement, we found that the PL lifetime of the PeSC with the paired EDLs was significantly shortened based on the average time-constant (τ_{ave}) which decreased from 23.8 (PeSC without EDLs) to 10.6 ns (PeSCs with the paired EDLs). Based on the PL measurements, we concluded that the paired EDLs lead to more efficient exciton dissociation and charge transfer by reinforcing E_{in} in the PeSC devices.

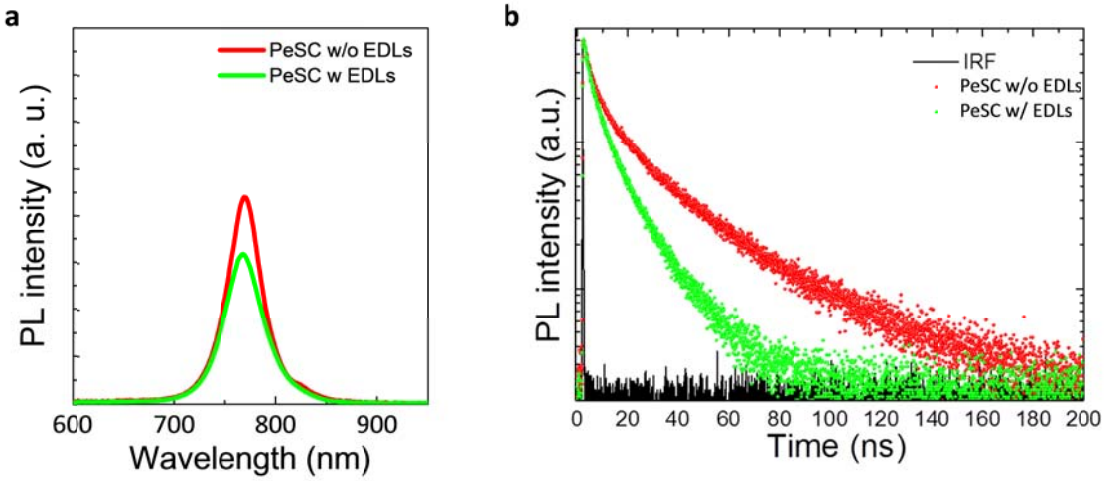

Figuer S8. (a) Steady state PL spectra and (b) PL decays for the PeSC devices with and without EDLs under short circuit conditions.

Table S6. Summary of parameters calculated from the PL decay curves of PeSCs. Monitored wavelength was 770 nm. The PL decay curves were fitted by a bi-exponential function to investigate exciton dynamics in PeSCs. The intensity weighted average exciton lifetime (τ_{ave}) was $f_1\tau_1 + f_2\tau_2$, where f_1, and f_2 are fractional intensities and τ_1, and τ_2 are lifetimes.[3]

Device structure	τ_1 (f_1) (ns)	τ_2 (f_2) (ns)	χ^2	τ_{ave} (ns)
w/o ELDs	30.78 (0.72)	5.85 (0.28)	1.272	23.80
w/ paired EDLs	14.52 (0.64)	3.71 (0.36)	1.180	10.63

10. Device stability in ambient air

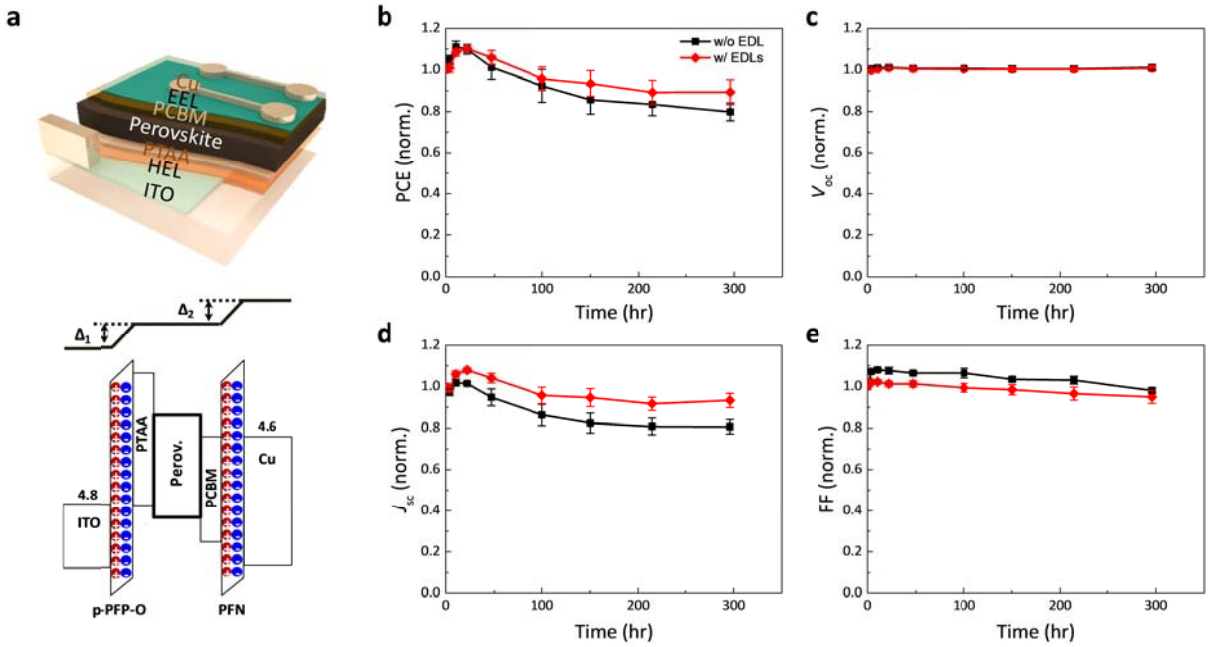

Figure S9. (a) Schematic illustration of device structure and energy level diagram of PeSCs with paired EDLs. Cu was used as a cathode to exclude the effect of chemical interaction with perovskite layer on the device air-stability. (b-e) Device performance variations with storage time under air (room temperature and relative humidity ~ 30%); (b) PCE, (c) *V*oc, (d) *J*sc, and (e) FF.

11. Effect of CPEs' thicknesses on device performance

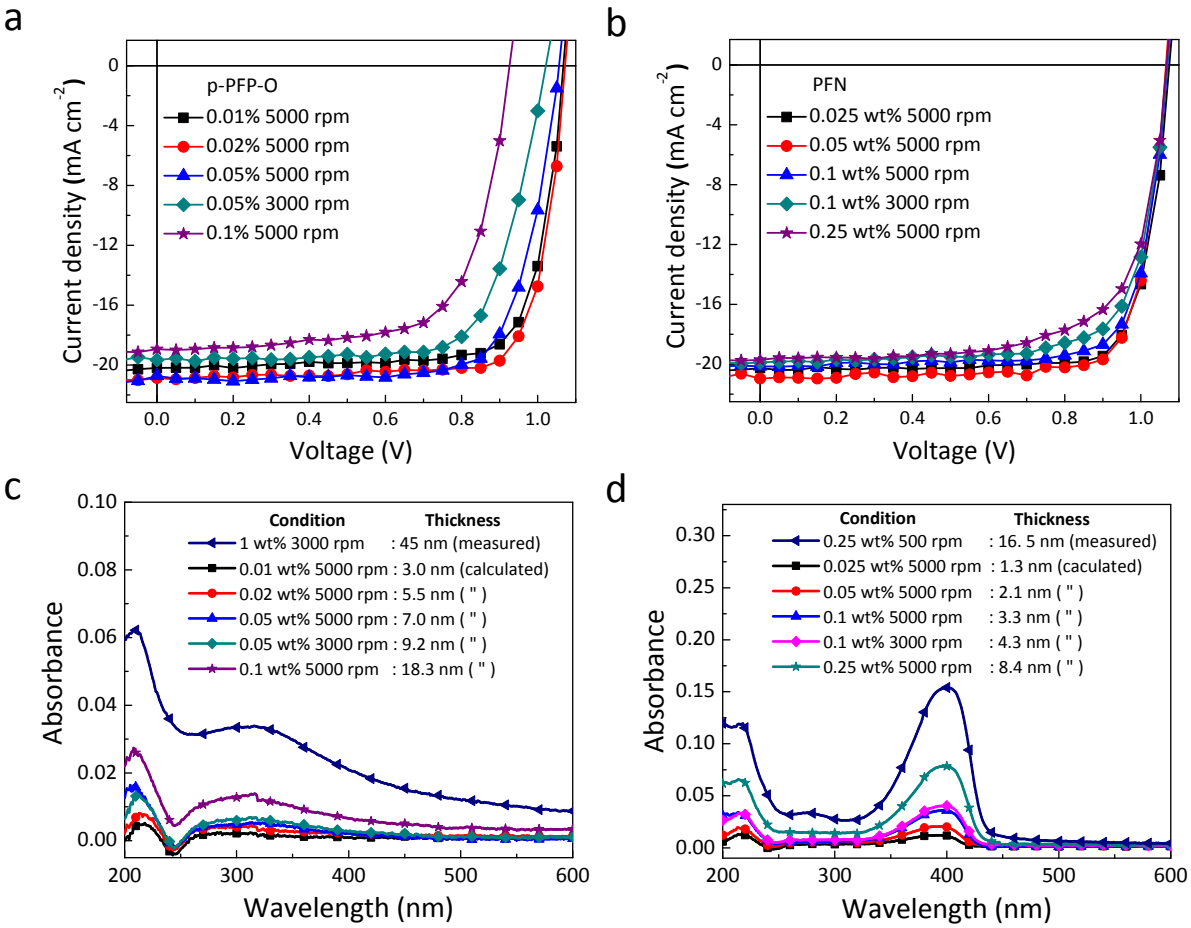

Figure S10. *J-V* characteristics of the PeSCs with the paired EDLs with various thicknesses. (a) p-PFP-O with various thicknesses from 3.0 to ~18.3 nm (PFN ~ 2 nm) and (b) PFN with thicknesses from 1.3 to 8.4 nm (p-PFP-O ~ 5.5 nm). (c, d) Absorbance spectra of (c) p-PFP-O and (d) PFN with different coating conditions. The thicknesses of the p-PFP-O and PFN films were estimated by calculating their relative absorbance ratio at a certain wavelength by comparing those of the films with already-known thicknesses.

Table S7. Performance parameters of PeSCs with respect to thickness of the p-PFP-O layer.

	Thickness (nm)	V_{oc} (V)	J_{sc} (mA cm^{-2})	FF	PCE (%)	R_s[a] (Ω cm^2)	R_{sh}[b] ($\times 10^3$ Ω cm^2)
p-PFP-O	3.0	1.07	20.20	0.78	16.8	4.17	1.19
	5.5	1.07	20.87	0.79	17.7	4.28	1.21
	7.0	1.06	20.73	0.76	16.6	5.28	1.16
	9.2	1.02	19.66	0.72	14.5	9.00	1.15
	18.3	0.93	18.94	0.69	12.1	10.22	0.87

[a]R_s: series resistance, [b]R_{sh}: shunt resistance

Table S8. Performance parameters of PeSCs with respect to thickness of the PFN layer.

	Thickness (nm)	V_{oc} (V)	J_{sc} (mA cm^{-2})	FF	PCE (%)	R_s (Ω cm^2)	R_{sh} ($\times 10^3$ Ω cm^2)
PFN	1.3	1.07	20.25	0.80	17.5	4.34	1.72
	2.1	1.07	20.96	0.79	17.7	4.55	1.67
	3.3	1.07	20.14	0.78	16.8	5.6	1.52
	4.3	1.07	19.87	0.75	15.9	6.35	1.39
	8.4	1.07	19.72	0.70	14.7	6.34	1.23

12. Device performance and reproducibility of PeSCs with various top electrodes

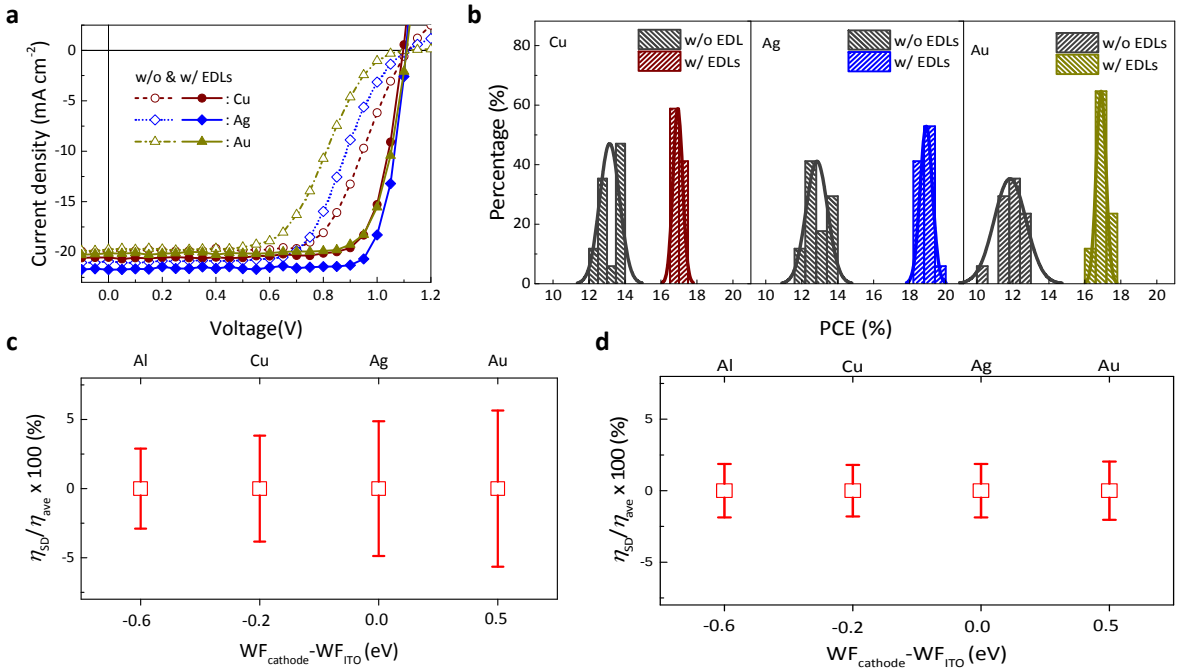

Figure S11. Device performance of PeSCs with various cathode electrodes. (a) *J-V* characteristics (b) PCE histograms of the devices without and with paired EDLs. (c-d) Device performance deviation from the average PCE ($\eta_{SD}/\eta_{ave,}$ where η_{SD} and η_{ave} are standard deviation and average values of PCEs) with respect to ΔWF (= $WF_{cathode}$-WF_{ITO}); The PeSC devices without (c) and with paired EDLs (d). In this experiment, to exclude the effects of solution batches of each material (p-PFP-O, PTAA, Perovskite, PCBM and PFN) on the performance variation, one solution batches of each material were used for the device fabrication.

Table S9. Performance parameters of PeSCs with various cathode electrodes. All reported solar cell parameters are the best values achieved among 17 devices of each type. The numbers in parentheses are the average values for all devices.

Cathode	*EDLs*	V_{oc} (V)	J_{sc} (mA cm^{-2})	FF	PCE (%)	$\eta_{SD}/\eta_{average}$ ×100 (%)
Cu	X	1.11	19.50	0.65	13.9 (13.2)	3.83
	O	1.11	20.53	0.78	17.6 (16.9)	1.87
Ag	X	1.11	20.20	0.60	13.7 (12.8)	4.88
	O	1.11	21.74	0.82	19.6 (18.9)	1.80
Au	X	1.12	19.75	0.57	12.7 (11.8)	5.66
	O	1.12	20.40	0.79	17.8 (16.9)	1.87

13. Nyquist plots of PeSCs

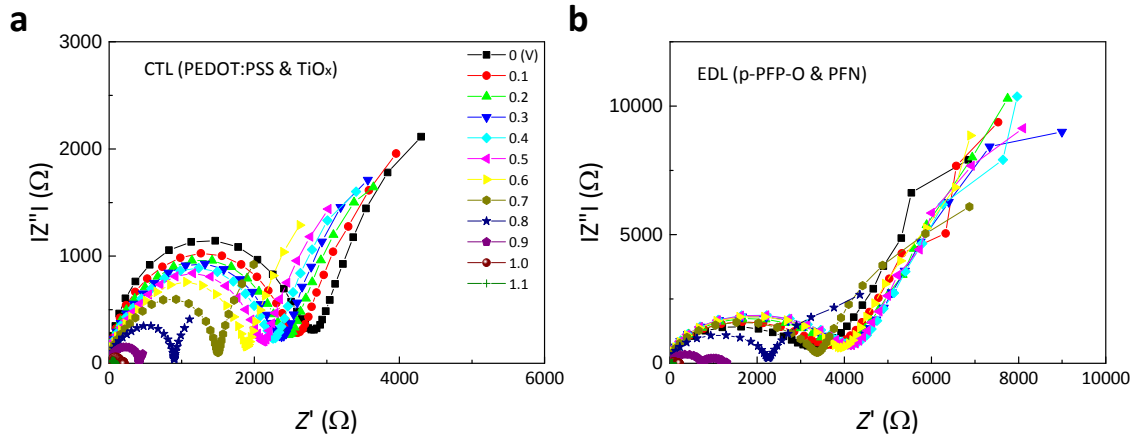

Figure S12. Nyquist plots of PeSCs with paired (a) CTLs and (b) EDLs measured under 1-sun illumination (frequency: 1 MHz ~ 10 Hz and voltage: 0 ~ 1.1 V).

Reference

[1]. B. H. Lee, J.-H. Lee, S. Y. Jeong, S. B. Park, S. H. Lee and K. Lee, *Adv. Energy Mater.* **2015**, *5*, 1401653.

[2]. J.-H. Lee, B. H. Lee, S. Y. Jeong, S. B. Park, G. Kim, S. H. Lee and K. Lee, *Adv. Energy Mater.* **2015**, *5*, 1501292.

[3]. R. W. K. Leung, S.-C. A. Yeh and Q. Fang, *Biomed. Opt. Express.* **2011**, *2*, 2517.